STAR
Research Journal

Available online at www.starresearchjournal.com (Star International Journal)

PHYSICS

CHARACTERIZATIONS OF Sno_2 NANO MATERIAL TOWARDS OPTO-ELECTRONIC PROPERTIES USING MORPHOLOGICAL AND OPTICAL TOOLS

S. LAVANYA[1] & Dr. M.K. MURALI[2]

[1]*Ph.D Scholar, Department of Physics, J.J. College of Arts and Science, Pudukkottai, Tamilnadu, India.*
[2]*Assistant Professor & Head, Department of Physics, J.J. College of Arts and Science, Pudukkottai, Tamilnadu, India.*

Abstract

In this attempt, nanometrically pure and singe phase adopted SnO_2 Nano material was prepared using popular sol-gel combustion route. The XRD measurements were carried out for comparing the calculated geometrical parameters with observed morphological results. The obtained XRD results proved the confined crystal structure of SnO_2 and related optimized molecular structure was predicted. The active planes were identified and the XR reflections were validated with respect to corresponding planes. The particle size was measured from the observed data and it was validated from the calculated results. The nano view of crystal structure was displayed using SEM tool and it was ensured from the obtained pictures of TEM. The direct and indirect band gap (kubo gap) of materials was evaluated and it was compared with calculated data. The annealing temperature effect was observed at 200º, 400º and 600ºC respectively of the nano samples. The XPS data was recovered from the nano samples and the corresponding energy dispersion graph was viewed. The photoluminescence spectral pattern was displayed and the shift of pattern was keenly monitored and cause of shift was recognized.

Keywords: SnO_2, XR reflections, SEM, Photoluminescence, Kubo gap.

1. INTRODUCTION

The inertial adoption of O on nano Sn lattice making the nano metal oxide n-type semiconductors which are having wide electronic and optical band gaps. Normally, such SnO_2 nano materials are having gas sensing characteristics [1-2] which are able to prepare sensitized solar cells, photo-voltaic devices and electronic catalyst [3-5]. Since SnO_2 nanostructures generally possess the translational symmetry, the SnO_2 nano materials specially contain the electronic, optical, opto-electronic and magnetic properties. In addition to that, due to its low dimensional, it can be possible to tailor the desired opto-electronic and micro molecular structural properties [6-7]. In common, the sol-gel combustion technique is mostly used to prepare the nano- SnO_2 since this method is convenient to manipulate the size and morphology of the resultant nanostructures [8]. The annealing temperature is normally used to reduce the size of the materials and improve the crystallinity which facilitates precise chemical reactions.

The SnO_2 is a popular and fascinate translucent conducting metal oxide which has a wide band gap, outsized exciton binding energy, high energy electronic-conductivity and considerable optical transparency [9-10]. The nano metal oxide SnO_2 is an economic, eco-friendly, chemically most stable metal oxide material which has high-quality reproductivities. Accordingly, the SnO_2 nano material behaves familiar nano materials for the purpose of preparation of solar devices, toxic gas sensors, LED display devices and lithium batteries. Hence, the nano sized tin oxide is capable material to have physicochemical properties to fabricate chemical sensors for determining the leakage of poisoned gases.

After the reviewing of previous research works on SnO_2, Even though the SnO_2 nano material having invariable applications in different field of nano industry, it was not characterized properly to observe the opto-electronic properties and other related physic-chemical and optical characteristics. In this work, the nano SnO_2 material was prepared and the samples were annealed at different temperatures and also they were characterized keenly.

2. EXPERIMENTAL METHODS

2.1. SYNTHESIS OF SnO_2

The SnO_2 crystalline solid has been converted in to nano crystalline by using sol-gel combustion process. For that, the Nitric acid was used to initiate oxidizing ions, whereas urea was acted as the fuel material. The aqueous form of solutions of pure metallic Sn was dissolved in nitric acid (72%, Merck) and for the attainment of stoichiometric ratio, the fuel urea (Merck) and deionised water were prepared. The pyrex vessel contained solution was heated under constant rousing at a temperature region of 90º-100°C and the concentrated solutions was slowly cooled without producing any precipitation until it turned into a white viscous gel. The portions of the gels were heated at temperature up to 350°C, which undergoes a strong self spreading

combustion reaction with the evolution of huge content of gases. The whole combustion process was completed in few minutes. The resulting yellow ruins was then calcined at 200º, 400º and 600°C respectively for eliminating the carbonaceous residues as shown in flowchart Figure 1[11].

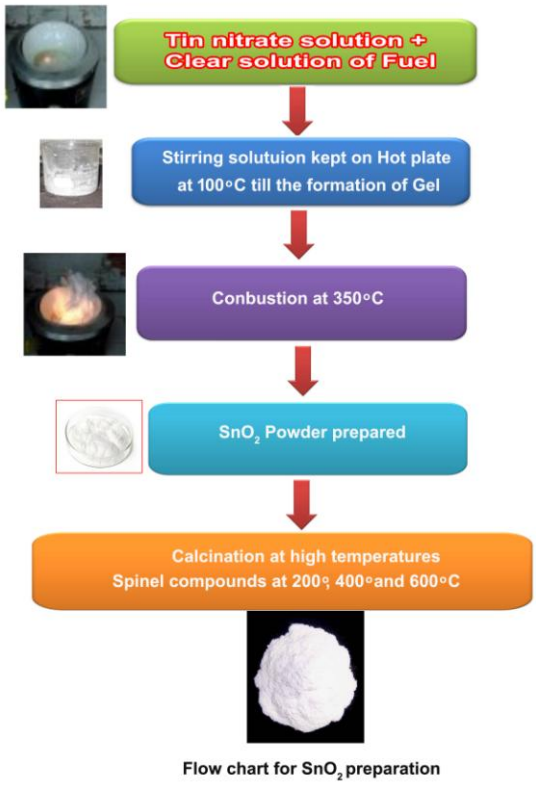

FIGURE 1
FLOW CHART FOR SnO_2 PREPARATION

In the combustion process using a fuel, the carbon and hydrogen atoms combined with oxygen and the heat with exponential rate was liberated which causing the rearrangement of valence electrons in Sn atoms resulting in the formation of new compounds.

Fuel + $O_2 \rightarrow$ Products + heat

According to Cooper et al., the oxygen balance of the reaction was defined in the field of propellants as in following expression:

$$OB\% = 100 \times \frac{AW_{oxygen}}{FW_{mixture}} 2\gamma O_2$$

where AW and FW are atomic weight of oxygen respectively and the formula weight of the mixture, γO_2 is the molar number of oxygen. In this case, three modes of Combustion [12] can be categorized depending on the value of OB.

This mode operated on the fuels/oxidizer ratio and was used to determine the reactivity of the reaction (explosive or moderate reaction). It is clear that, the fuel to oxidizers ratio affects the total surface area of the product powder and then the particle size of the final products.

3. RESULTS AND DISCUSSION

3.1. XRD ANALYSIS

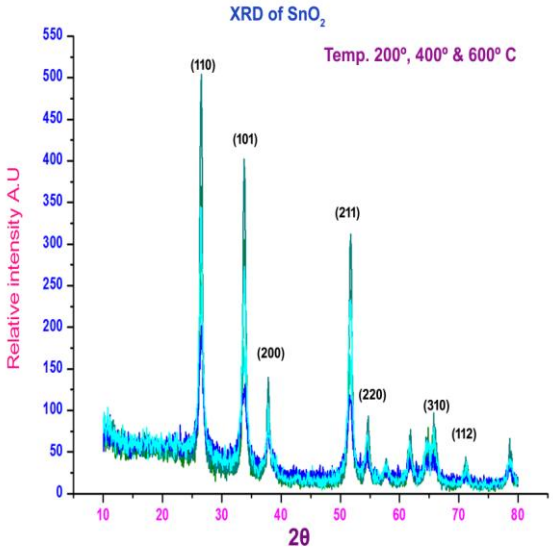

FIGURE 2
XRD SPECTRAL OF SnO_2

According to the XRD spectral Figure-2, the intensive peaks were obtained from the active planes of SnO_2. For the raw prepared SnO_2, the diffractional peaks were observed from (110), (101), (200), (211), (220), (310) and (112) interplanes and were found to be agreed well with the JCPDS data of the card No. 77-0452. The observed data associated with the nano compound under study was supported by the previous work [13]. The locations of the diffraction signals belong to the rutile tetragonal SnO_2 structure. The sample was annealed at 200º, 400º and 600 º C temperatures respectively and the peaks were also being found in the same figure. Here, the peak intensity of prepared sample was found to be low whereas at 200º, 400º and 600 º C, the intensity of peaks were identified to be increased and at maximum temperature, the most intensive peaks were observed. From the obtained peaks with superior intensity showed that, when the temperature increases, the nano crystallinity become well in order. In this case, the peaks related to the planes were not moved instead of increment of intensity which clearly indicates that, the base lattice was not distorted due to the annealing effect. This proves that, the molecular structure was recognized as tetragonal symmetry which is consistent base lattice structure and this stabilized crystal was found to be very strong up to 600ºC according to this work.

TABLE 1
OPTIMIZED GEOMETRICAL PARAMETERS FOR SnO_2 COMPUTED AT HF AND DFT METHODS WITH 6-31G(d,p) BASIS SET

Geometrical Parameters	Methods	
	HF/6-31G(d,p)	B3LYP/6-31G(d,p)
Bond length(Å)		
(Sn1-O2)	1.984	1.983
(Sn1-O3)	2.128	2.128
(Sn1-O9)	2.112	2.117
(O2-Sn4)	1.930	1.934
(O3-Sn4)	2.022	2.028
(Sn5-O6)	2.046	2.041
(Sn5-O7)	1.914	1.912
(O6-Sn8)	3.134	3.131
(O6-O9)	1.482	1.484
(O7-Sn8)	1.965	1.965
(Sn8-O9)	2.161	2.168
Bond angle(˚)		
(O2-Sn1-O3)	73.986	73.983
(O2-Sn1-O9)	100.885	100.888
(O3-Sn1-O9)	70.852	70.857
(Sn1-O2-Sn4)	108.182	108.124
(Sn1-O3-Sn4)	99.566	99.564
(O2-Sn4-O3)	77.580	77.589
(O6-Sn5-O7)	87.047	87.037
(Sn5-O6-Sn8)	82.438	82.484
(Sn5-O6-O9)	111.959	111.991
(Sn5-O7-Sn8)	129.583	129.535
(O6-Sn8-O7)	59.576	59.578
(O7-Sn8-O9)	78.133	78.138
(Sn1-O9-O6)	109.763	109.768
(Sn1-O9-Sn8)	103.680	103.684
Dihedral angle(˚)		
(O3-Sn1-O2-Sn4)	-6.545	-6.546
(O9-Sn1-O2-Sn4)	-72.799	-72.794
(O2-Sn1-O3-Sn4)	6.016	6.015
(O9-Sn1-O3-Sn4)	113.933	113.931
(O2-Sn1-O9-O6)	-145.905	-145.915
(O2-Sn1-O9-Sn8)	87.859	87.853
(O3-Sn1-O9-O6)	145.452	145.454
(O3-Sn1-O9-Sn8)	19.214	19.214
(Sn1-O2-Sn4-O3)	6.781	6.782
(Sn1-O3-Sn4-O2)	-6.087	-6.082
(O7-Sn5-O6-Sn8)	6.565	6.565
(O7-Sn5-O6-O9)	-17.440	-17.448
(O6-Sn5-O7-Sn8)	-13.563	-13.567
(Sn5-O6-Sn8-O7)	-7.409	-7.408
(Sn5-O6-O9-Sn1)	-76.803	-76.808
(Sn5-O7-Sn8-O6)	10.213	10.214
(Sn5-O7-Sn8-O9)	28.016	28.019
(O7-Sn8-O9-Sn1)	82.321	82.322

TABLE 2
CRYSTAL PARAMETERS OF SnO_2

Parameters	Prepared	200 °C	400 °C	600 °C
a (Å)	4.750	4.684	4.649	4.537
c (Å)	3.172	3.175	3.178	3.186
Crystal size (nm)	42.03	36.78	34.11	30.14
Cell mass	249.94	244.49	244.52	244.53
Cell volume ($Å^3$)	71.986	70.867	71.718	71.699
Crystal density (g/cm^3)	5.870	6.364	6.458	6.499
R-Bragg	2.686	2.697	2.768	2.857
R_{wp}	16.30	16.56	18.06	17.02
Goodness of fit (GOF)	1.01	1.05	1.12	1.08

The SnO_2 nano crystal size (D) was calculated from line broadening examination linked with observed diffraction peaks by Scherer expression. The predicted average crystallite size is in the nanometer scale was found to be 42.03nm for prepared nano sample which was appeared to be decreased up to 30.14 nm by the application of annealing temperature up to 600ºC. In this case, according to the observed peaks, the lattice constant 'a' decreases from 4.750 to 4.537 Å whereas 'c' increases from 3.172 to 3.186 Å. Such the observed data appeared to be well agreed with metal oxides nano particles. This view showed the lattice expansion with the reduction of micro-strain and dislocation density.

From the Raman scattering peaks, it was observed that, the fundamental Raman peaks at 632 and 679 cm^{-1} were strongly represented the by mode of the transverse optical phonons associated with rutile lattice. These Vibrational modes assigned approved by the polarization of Sn-O bonds existed in rutile SnO_2 and it was in line with the literature [14]. According to the relaxation of the k ¼ 0 selection rule, when the rate of disorder increases or the nano particle size decreases, the structural distortion induced. Generally, when the crystallite is reduced to nano scale, the phonon scattering could not be controlled by center of the Brillouin zone. Here, since the distortion taking place in particle size, the crystal symmetry becomes visible. From the above discussion, it was inferred that, the particle size was reduced by the application of the temperatures and due to this; the micro-strain was further reduced and the crystal order gradient was improved much.

The goodness of fit value is very precise to illustrate whether the obtained data consistent or not. Accordingly, in this case it was ranged from 1.01 to 1.12 which showed the acquired data was found to be within the expected value. Its crystal density was ranged from 5.870 to 6.499 g/cm^3 of sample as in preparation to annealed temperature about 600ºC respectively. It was good fit with pubchem data of centralized standard unit. The cell volume was found to be decreased from 71.98 to 71.69 which ensured the increment of packing fractions. The R-Bragg value of samples calculated from 2.686 to 2.857 which exposed the rather deviation of the observed reflection intensities from calculated results.

3.2. SEM INVESTIGATION

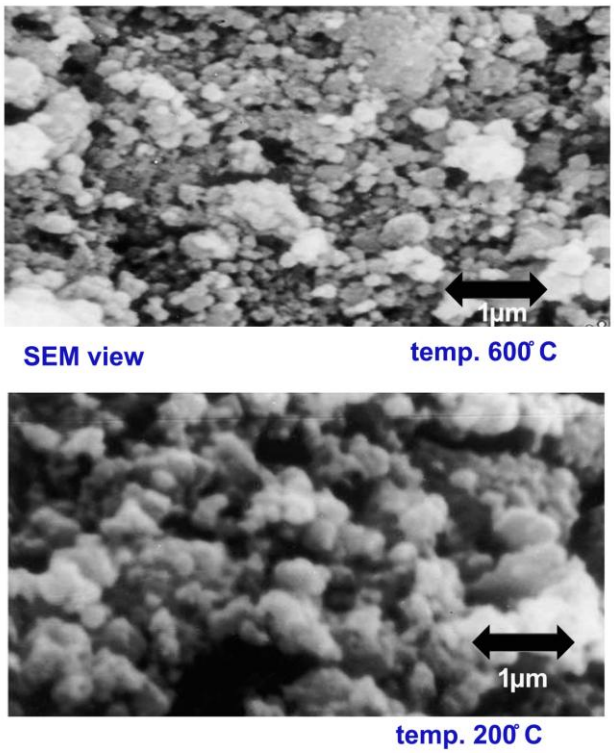

FIGURE 3
SEM VIEW OF PRESENT CASE WITH ANNEALING TEMPERATURES

The SEM view of present case with annealing temperatures was presented in the Figure -3 in which the clear morphological view was clearly seen. The view was magnified up to 1µm by which the roughed surface of the SnO_2 crystal was remarkably observed. The dullness surface of prepared material was displayed by SEM view at 200ºC where, the coarse metal oxide was seen. The annealing temperature at 600ºC, the improved surface was appeared which was also come in to view on same figure. From these figures, it was noted that, the annealing process improve the smoothness of the surface and it helped to produce significant material property. The SEM also illustrated that, the ineptness of the surface indirectly showed the rigidness of the SnO_2 nano crystal. Such a porosity surface is very significant to absorb the gas in different pressure and it is also capable to receive the light energy with low reflection coefficient.

The SEM usually used to study the grain appearance and grain boundary characteristics and thereby determining the conducting ability. Here, the positive gradient of roughness of surface creating advanced diffusion coefficient in the nano crystalline state. Therefore, the fine grain boundaries are usually anticipated to demonstrate the sensitive conductivity [15]. In this case, the favorable discrete grain boundaries causing porosity of the material and it is able to conduct with higher magnitude.

3.2. TEM ANALYSIS

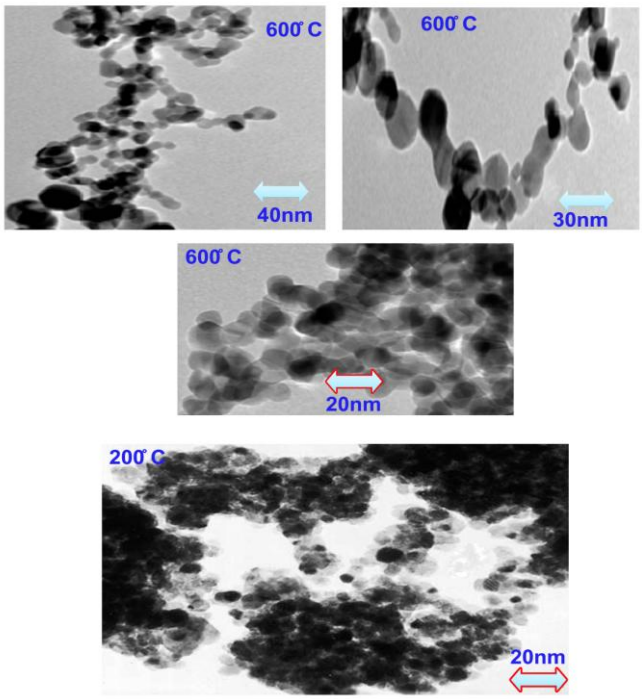

FIGURE 4
TEM PHOTOGRAPH

The TEM view of the nano samples used to study the particle size and morphology of the materials [16]. The TEM photograph of the present case was depicted in the Figure-4. The TEM view of present SnO_2 samples annealed at different temperatures was displayed in the Figure 4 in which different magnifications were recorded. The TEM pictures were captured in 20 nm at 200º and 600ºC and the depth pictures were captured in 30 and 40 nm at 600ºC. After the refinement of active hkl plane at (110) with higher reflection coefficients, the particle view was mapped and the clear diagram was obtained. The observed diagram showed the spherical shape of nano particle with transparent grain boundary. At the annealing temperature 200ºC, the size can be predicted from the photograph and not to be confined properly whereas at 600ºC, the particles were seen clearly and the boundaries can be estimated properly. The TEM also ensued that, the crystallinity was improved from 200º to 600º C in good order and the observed pattern confirmed the presence of ultrafine crystals. Apart from that, the chain of nano particles was appeared and the chain was connected interactively.

3.3. OPTICAL ANALYSIS: UV-Vis ANALYSIS

The optical property is directly related with optical transparency of the prepared nano materials. The

connection between the absorption coefficient and optical band gap is articulated as,

$$\alpha h \upsilon = A (h \upsilon - E_g)^{1/n}$$

In this case, α is the absorption coefficient analogous to frequency υ and Eg is a band gap energy. The constant n denotes the nature of electronic transition. The SnO_2 have direct permissible transition and hence n is equal to 2. The optical band gaps of SnO_2 was determined by extrapolating the linear section of the curve from the plot of $(\alpha h\upsilon)^2$ versus hυ. For allowed transition α^2 is plotted against energy (E = h υ) to acquire a straight line for direct transitions which was shown in Figure-5 where in which the band gap was determined. In this case, the obtained optical band gap values showed the little variation from 3.460 to 3.289 eV, for the prepared and annealed at 600 ºC which was depicted in the Table-3.

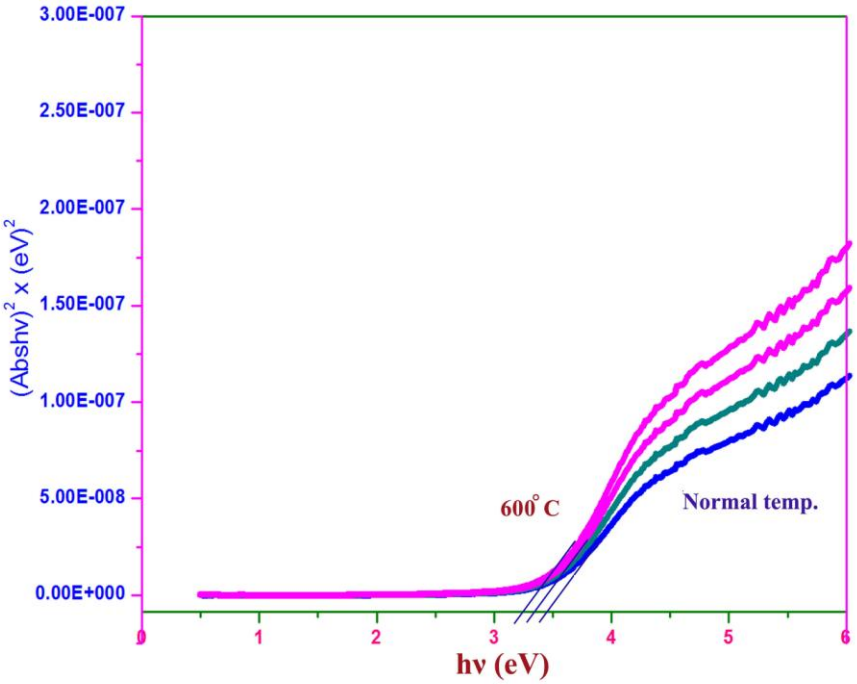

FIGURE 5
STRAIGHT LINE FOR DIRECT TRANSITIONS

TABLE 3
UV-Vis BAND GAP VALUES AND (PL) BAND GAP VALUES OF SnO_2 FROM 200°- 600°C

SnO_2	prepared	200° C	400° C	600°C
UV-Vis E_g (eV)	3.965	3.750	3.630	3.460
(PL) E_g (eV)	3.735	3.679	3.615	3.289

While the annealing temperature is increased from 200 to 600º C, the band gap was found to be increased due to decreasing of crystallite size. When annealing temperature increases, the grain sizes become small and thereby the density of nano particles grain boundary reduces and therefore the number of trapped carriers is less which makes the availability of higher amount of charge carriers for optical conduction. This kind of variation in carrier concentration guides a modification in the optical band gap of disintegrated nano semiconducting material which is represented as:

$$E_g - E_{go} = \Delta E_{gBM} = \frac{h}{2m^*}\left(3\pi^2 n_e\right)^{2/3}$$

Here, the Ego is the intrinsic band gap, m* is the electron effective mass and ne number of carrier concentration.

By the application of annealing temperatures, the band gap for the SnO_2 nano material was determined to be decreased which was attributed by oxygen shortage and correspondingly the carrier concentration of SnO_2 nano particles gets reduced since the creation of acceptor

kind non-stoichiometric defects produced. The annealing effect also causing the compensation centers in the material. Generally, the optical reflectance is very important in evaluating the optical performance of conducting metal oxide particles. An optical reflection spectrum of SnO_2 at normal and annealing temperatures were presented in the Figure-6. From the Figure, it was important to note that, the optical reflection decrement was taking place due to subsurface scattering and the roughness of the surface of the nano material.

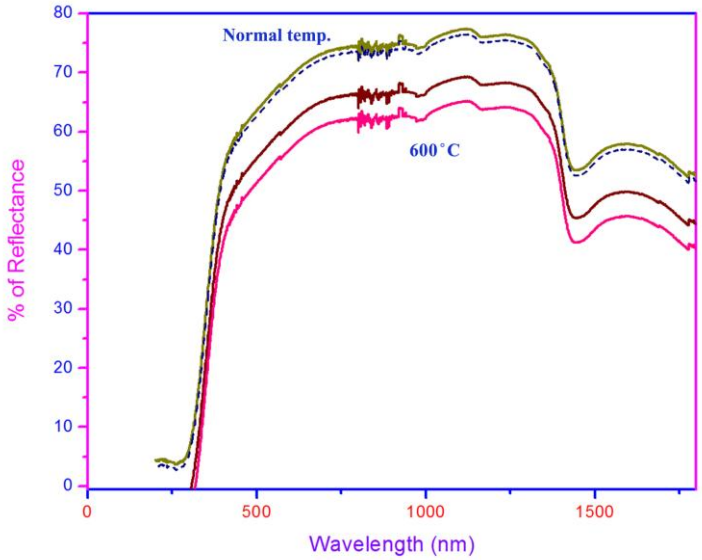

FIGURE 6
AN OPTICAL REFLECTION SPECTRUM OF SnO_2 At Normal And Annealing Temperatures

When the nano material is annealed with higher temperature, a sharp optical reflection is taking place at the curve. It directly indicates a improved larger crystallinity of the particles and inferior carrier density close to the band edge. Furthermore, there was a shift found in absorption edge to shorter wavelength with increasing annealing temperature which was also due to the Burstein Moss shift [17-18].

3.7 PHOTOLUMINESCENCE ANALYSIS

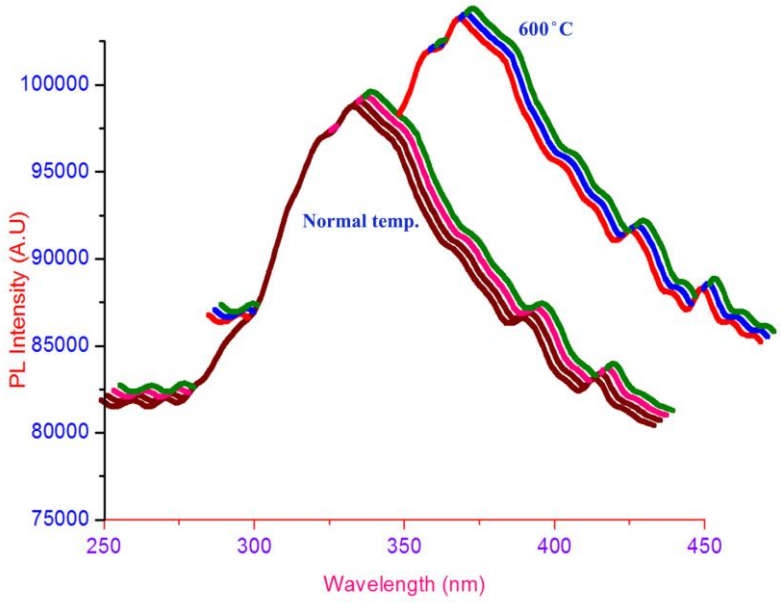

FIGURE 7
PL SPECTRA Of SnO_2

The Photoluminescence spectrum for the nano materials is convenient to investigate the distortion of morphological structure due to defect and the level of impurity can be measured accurately [19]. The PL spectra of the present material with different temperatures were displayed in the Figure-7 in which the excitonic photoemissions were clearly shown. Here, the excitation wavelength used for the PL measurements ranged from 250 nm to 470 nm. The peak intensity is usually inversely proportional to the size of the nano particles. The intensive peaks were obtained at 3.73 eV with 330 nm for prepared sample whereas the associated peaks were observed at 3.67, 3.61 and 3.28 with absorption wavelength 365, 368 and 372 nm respectively for the sample annealed at 600ºC. This was mainly by the application of photo-excited electrons undergoing non-radiative thermal scattering processes before organizing electron-hole pairs. It was also due to assembly of oxygen vacancies which may be acted as radiative centers in photoluminescence emission processes. From the above discussion, it was concluded that, due to the influence of annealing temperatures, the PL intensity was found to be increased and at the same time, the wavelength shift was observed towards blue region of visible range.

4. CONCLUSION

The SnO_2 nano powder was prepared by sol-gel combustion process and the prepared sample was annealed with discrete levels of temperatures such as 200º, 400º and 600º respectively. Each and every annealed temperature point, the sample was keenly characterized. From the morphological test, the SnO_2 nano material was able to sense the toxic gases due to its nano grain boundary micro-amalgamated structure. The SEM results of the samples were supported the morphological roughness of the material and the TEM profile defined the grain boundaries well. The shape structure of nano particles were studied with respect to the annealing temperatures. The optical analysis has been carried out from which the optical band gap was estimated in the range of 3.480 - 3.287 eV. The annealing effect was observed in the optical band gap from higher level to rather optimized level. The annealing temperatures resized the optical sensitivity and it was able to receive the visible energy and reproduce in the form of electrical signal. The PL studies for the SnO_2 nano materials were carried out and the results demonstrated the PL performance shifting to the another part of UV-Visible region of the spectrum.

REFERENCES

1. G. Lu, L.E. Ocola, J. Adv. Mater., 21 (2009) 2487−2491.
2. M. D'Arienzo, L. Armelao, A. Cacciamani, C.M. Mari, S. Polizzi, R. Ruffo, R. Scotti, A.Testino, L. Wahba, F. Morazzoni, Chem. Mater., 22 (2010) 4083–4089.
3. J.F. Qian, P. Liu, Y. Xiao, Y. Jiang, Y.L. Cao, X.P. Ai, H.X. Yang, Adv. Mater. 21 (2009) 3663–3667.
4. C. Prasittichai, J.T. Hupp, J. Phys. Chem. Lett. 1 (2010) 1611–1615.
5. H.J. Snaith, A. Stavrinadis, P. Docampo, A.A.R. Watt, Sol. Energy 85 (2011) 1283–1290.
6. V. Kumar, A. Govind, R. Nagarajan, Inorg.Chem. 50 (2011) 5637–5645.
7. S. Wu, S. Yuan, L. Shi, Y. Zhao, J. Fang, J. Colloid Interface Sci. 346, (2010) 12–16.
8. W.D. Shi, S.Y. Song, H. Zhang, J. Chem. Soc. Rev. 42 (2013) 5714–5743.
9. Y. Masuda, K. Kato, Thin Solid Films, 544, (2013) 567.
10. T. Tharsika, A.S.M.A. Haseeb, M.F.M. Sabri, Thin Solid Films, 558, (2014), 283-288.
11. N.Y. Shishkin, I.M. Zharsky, V.G. Lugin, V.G. Zarapin, Sensors and Actuators; B 48, (1998) 403.
12. T. Hanrath and B. A. Korgel, Journal of American Chemical Society; B, 124, (2002) 1424–1429.
13. F.C. Vasquez, F. Paraguay-Delgado, J.E. Morales-Mendoza, W. Antúnez-Flores, D. A.Lardizabal, G. Alonso-Nuñez, G. Berhault, Superlattices and Microstructures, 90, (2016), 274-287.
14. C.G. Granqvist, A. Hultaker, Thin Solid Films, 411, (2002), 1, 22, 1-5.
15. A. Chandra Bose, D. Kalpana, P. Thangadurai, S. Ramasamy, Journal of Power Sources, 107 (2002) 138–141.
16. M. John Silvister Raju, S.S. Bhattacharya, Materials Today: Proceedings, 5, (2018), 10097-10103.
17. C Huang; Z Tang; Z Zhang; J Am. C. Huang, Z. Tang, Z. Zhang, J. Am. Cerm. Soc. 84 (2001) 1637, 335.
18. M. Girtan, G.I. Rusu, G.G. Rusu, S. Gurlui. Applied surface science 162, (2000), 492- 498.
19. S. I. Najafi, Introduction to Glass Integrated Optics, Artech House, Norwood, MA, (1992).